steel research international
www.steel-research.de

Kinetic Mechanism Development for the Direct Reduction of Single Hematite Pellets in H_2/CO Atmospheres

Mohammed Liaket Ali, Quentin Fradet, and Uwe Riedel*

Increasing interest in the direct reduction process of iron ore has revived investigations on gaseous and heterogeneous iron oxides' kinetics. Despite extensive studies on the reduction of iron oxides with pure hydrogen or syngas, the development of a generic reduction mechanism for iron oxides is still lacking. The conventional shrinking core model hardly distinguishes between transport and reaction processes, leading to biases or even errors in the kinetic models. In the present study, a porous solid model, which solves mass balances of the individual gas-phase species and solid ones assuming spherical symmetry, is used for developing a heterogeneous kinetic mechanism accounting for different iron oxidation stages (Fe_2O_3, Fe_3O_4, FeO). It also accounts for carbon accumulation and cementite formation to model the carburization phenomena when using carbon-containing reducing agents like syngas. The proposed generic mechanism successfully reproduces 49 experimental data sets from the literature for single iron oxide pellets' isothermal reduction with syngas of varying hydrogen content up to pure hydrogen without any adjustment of its parameters. The model predictions are in excellent agreement with the experimental data. Finally, the carburization kinetics are explained, and the factors (e.g., temperature, hydrogen content) affecting the carbon deposition are analyzed.

1. Introduction

The steel industry currently faces significant challenges. These are enormous environmental impacts, material usage, energy consumption, and byproducts of the processes.[1] In 2020, the total crude steel production was 1869 million tons (Mt).[2] The conventional blast furnace-basic oxygen furnace (BF-BOF) route produces 70% of the global crude steel,[3] utilizing coke to produce iron by reducing iron ore, which emits high amounts of CO_2 in the environment. Steel production contributed 6.7% of the global anthropogenic emissions of CO_2 in 2020, and the average emission is estimated to be 1.8 t CO_2/ per t steel.[4] This corresponds to ≈3.46 Gt CO_2 per year, eventually leading to even higher annual emissions in 2050 due to the growing steel demand. Given this high level of CO_2 emissions, steel production cannot rely on continuous process optimization but instead, needs fundamental technological changes to meet future emission limitations.

Under these circumstances, the direct reduction (DR) process of iron oxide is a promising technology to reduce the CO_2 emissions where hematite (Fe_2O_3) is reduced by syngas (H_2/CO-mixture) or even with pure hydrogen (H_2). Many mathematical models have been proposed in the literature to predict the gaseous reduction behavior of iron oxide. However, due to a large number of influencing factors in the direct reduction process, for example, gas composition, operating pressure, temperature, or solid material characteristics (porosity, tortuosity, grain size, gangue contents, mineralogy, etc.), uncertainty is relatively high. Researchers usually try to balance between model simplicity and accuracy (agreement with experimental data). To avoid the inherent complexity of the direct reduction process, McKewan[5] developed a simple one-interface shrinking core model by considering the interface chemical reaction as the rate-limiting step. They concluded while validating against their data that diffusion and chemical reaction should be considered simultaneously. Tsay et al.[6] developed a model based on a three-interface shrinking core model for H_2/CO mixtures, considering the same diffusivities and mass transfers for reactants and products. However, this approach has the evident weakness of assuming a distinct sharp interface between different solid oxides. A transient isothermal model based on the grain model has been proposed by Valipour et al.[7] to simulate a porous hematite pellet's thermal and kinetic behavior in a syngas environment. They showed how models not considering the film resistances deviate systematically from the experimental data.

Aside from the fundamental mathematical approach, the chemical kinetics of reduction of iron oxide with H_2/CO mixtures has not been adequately investigated, especially the carbon deposition phenomena. Turkdogan et al.[8] studied the kinetics of direct reduction process of iron oxide using hydrogen. They found out that the transformation process of hematite to iron is mediated by magnetite (Fe_3O_4) and wüstite ($Fe_{(1-y)}O$).

M. L. Ali
German Aerospace Center (DLR)
Institute of Low-Carbon Industrial Processes
Schwenninger Weg 1, 02763 Zittau, Germany
E-mail: mohammed.ali@dlr.de

Q. Fradet, U. Riedel
German Aerospace Center (DLR)
Institute of Low-Carbon Industrial Processes
Walther-Pauer-Straße 5, 03046 Cottbus, Germany

The ORCID identification number(s) for the author(s) of this article can be found under https://doi.org/10.1002/srin.202200043.

DOI: 10.1002/srin.202200043

Hai-bin et al.[9] investigated the controlling steps of the iron oxide reduction kinetics with H_2/CO-mixtures and concluded that the process is initially interfacial chemical reaction controlled and later shifts to a diffusion-controlled or mixed regime. Mousa et al.[10] studied the isothermal reduction of iron oxide with simulated original and reformed coke oven gas in the temperature range from 973 to 1253 K. They mentioned the cracking of CH_4 into carbon and H_2 at temperature above 973 K. Furthermore, carbon deposition was observed at the later reduction stage with an increase in CH_4 content. Towhidi and Szekely[11] researched the effect of carbon deposition on the reduction kinetics of commercial-grade hematite pellets with CO, H_2, and N_2. Their results show that, below 1173 K and with H_2/CO-mixtures, the reduction process is accompanied by the carbon deposition process, and this carbon deposition is proportional to the CO content in the reducing gas. Xu et al.[12] showed that active Fe is a catalyst for carbon deposition reactions while diffusion is not a rate-controlling factor for CO decomposition.

Considering the previous works, the absence of a generic mathematical model which can reproduce the iron ore pellet reduction process for a wide range of experimental operating conditions becomes apparent. Most of the models perform satisfactorily in a narrow window of experimental conditions. To the best of the authors' knowledge, the number of available mathematical models gets even lower when it comes to predicting the reduction process with complex carbon deposition.

In this work, we propose a generic kinetic mechanism for the direct reduction process of a single hematite (Fe_2O_3) spherical pellet in a shaft reactor using H_2/CO as reducing gases. The concept of a porous solid pellet model has been considered, which defines mass fluxes of the reactant gases and pellet properties along the reduction process. The variation of the pellet porosity with time and the film resistance has been considered to make the model more robust. With the usual three-step heterogeneous iron oxide reduction reactions ($Fe_2O_3 \rightarrow Fe_3O_4 \rightarrow FeO \rightarrow Fe$), chemical kinetics of carburization is also considered. The scheme has been designed for atmospheric pressure operation and at a temperature range from 873 to 1507 K. This kinetic mechanism has been validated against comprehensive sets of available literature data. So the main goals of the present work can be summarized as 1) reproducing comprehensive sets of available experimental data from the literature to prove the robustness of the present model, 2) investigating the difference of using H_2, CO, and H_2/CO mixtures for the reduction process concerning the reduction kinetics and the associated chemical reactions, and 3) explaining the carburization kinetics and analyzing the probable factors (e.g., temperature, hydrogen content in the mixture) affecting the carbon deposition.

2. Kinetics and Thermodynamic Models of Gaseous Iron Oxide Reduction

2.1. Modeling Framework

The porous solid pellet model is adopted in this work as the basis for predicting the kinetic mechanism of the heterogeneous gaseous iron oxide reduction process. As in the reduction process, the chemical reactions and the gaseous diffusion occur simultaneously inside the pellet, the conventional shrinking core model is not an appropriate choice to investigate the chemical kinetics. The porous solid pellet model discretizes and solves gaseous and solid species variables along the radius of a spherical geometry. The model determines the evolution of the gas and solid species and can handle multiphase chemistry. The chemical source term and species transport through diffusion evolve with time. The basic equations are as follows

$$\frac{\partial \varepsilon C_i}{\partial t} = -\nabla \cdot (-D^{\text{eff}} \nabla C_i) + \dot{s}_i, \quad i \in \text{gas} - \text{gas species} \tag{1}$$

$$\frac{\partial (1-\varepsilon)\rho_j X_j}{\partial t} = M_j \dot{s}_j, \quad j \in \text{solid species} \tag{2}$$

In the following, the index i will be used for gaseous species and j for any solid species. The variables ε, C, D^{eff}, ρ, X, M, and $\dot{s}$ are respectively the porosity [%], the concentration [mol m^{-3}], the effective diffusivity [m^2 s^{-1}], the density [kg m^{-3}], the mole fraction [−], the molar weight [kg mol^{-1}], and the chemical source term [mol m^{-3} s^{-1}] of the surface reactions. For simplifying the derivatives of Equation (1) and (2), the properties $\sum_j X_j = 1$ and the density ρ_j, of the pure substance, is considered constant. After transformations, we obtain a set of equations comprising the temporal derivatives of each gas species, of each solid species, and of the pellet porosity.

$$\frac{\partial C_i}{\partial t} = \frac{1}{\varepsilon}\nabla \cdot (D^{\text{eff}} \nabla C_i) + \frac{1}{\varepsilon}\dot{s}_i - \frac{C_i}{\varepsilon}\frac{\partial \varepsilon}{\partial t} \tag{3}$$

$$\frac{\partial X_j}{\partial t} = \frac{1}{(1-\varepsilon)}\frac{M_j}{\rho_j}\dot{s}_j + \frac{X_j}{(1-\varepsilon)}\frac{\partial \varepsilon}{\partial t} \tag{4}$$

$$\frac{\partial \varepsilon}{\partial t} = -\sum_j \frac{M_j}{\rho_j}\dot{s}_j \tag{5}$$

These equations are discretized along the pellet radius for a certain number of spatial points. A system of ordinary differential equations (ODEs) will be generated by this process. The detailed mathematical expressions and derivations of our model are discussed in another article.[13] This article gives further insights into the solution of the gas species concentrations and solid mole fractions along the pellet radius, assuming spherical symmetry.

2.2. Reaction Schemes

The gaseous reduction of hematite (Fe_2O_3) is a complex temperature-dependent process. Iron ore reduction undergoes the following sequence.

$$\begin{aligned} Fe_2O_3(\text{hematite}) \rightarrow Fe_3O_4(\text{magnetite}) \rightarrow FeO(\text{wüstite}) \\ \rightarrow Fe(\text{metallic iron}) \end{aligned} \tag{6}$$

Depending on the reducing gas concentration, temperature, and extent of reaction, the solid can be found in any of those states mentioned earlier. The chemical formula FeO is a simplified representation of wüstite. Reduction carried out at a temperature lower than 843 K will bypass the FeO (wüstite) from the sequence, as wüstite is unstable at this zone.[14] However, DR of iron ore pellets is usually performed at a higher temperature, involving wüstite. The time of completion of the last reduction states (FeO→Fe) is the slowest of all.[15]

The proposed kinetic scheme consists of 14 reactions, all of which are first-order reaction. Among them, 13 are heterogeneous and one is a homogeneous reaction (reaction 19). The chemical source term ($\dot{s}$) mentioned in 2.1 considers the solid species mole fractions and the gas species concentrations. The reduction chemistry of iron oxide to iron with pure hydrogen can be described with the following steps.

$$3\ Fe_2O_{3(s)} + H_{2(g)} \rightarrow 2\ Fe_3O_{4(s)} + H_2O_{(g)} \quad (7)$$

$$Fe_3O_{4(s)} + H_{2(g)} \leftrightarrow 3\ FeO_{(s)} + H_2O_{(g)} \quad (8)$$

$$FeO_{(s)} + H_{2(g)} \leftrightarrow Fe_{(s)} + H_2O_{(g)} \quad (9)$$

Equation (7) is exothermic in nature, whereas Equation (8) and (9) are endothermic. This could indicate why the reduction of iron ore consisting of Fe_2O_3 is usually faster than the one with only Fe_3O_4.[14]

Reduction with CO and C follows similar three-step reactions as the reduction with hydrogen.

$$3\ Fe_2O_{3(s)} + CO_{(g)} \rightarrow 2\ Fe_3O_{4(s)} + CO_{2(g)} \quad (10)$$

$$Fe_3O_{4(s)} + CO_{(g)} \leftrightarrow 3\ FeO_{(s)} + CO_{2(g)} \quad (11)$$

$$FeO_{(s)} + CO_{(g)} \leftrightarrow Fe_{(s)} + CO_{2(g)} \quad (12)$$

The C-reduction reactions complete the scheme.

$$3\ Fe_2O_{3(s)} + C_{(s)} \rightarrow 2\ Fe_3O_{4(s)} + CO_{(g)} \quad (13)$$

$$Fe_3O_{4(s)} + C_{(s)} \rightarrow 3\ FeO_{(s)} + CO_{(g)} \quad (14)$$

$$FeO_{(s)} + C_{(s)} \rightarrow Fe_{(s)} + CO_{(g)} \quad (15)$$

Now, considering the stoichiometry associated with these reactions, the theoretical weight loss in each of the states is shown in **Table 1**. This clearly shows that the maximum weight loss or removal of oxygen happens at the last stage.

The reduction in the presence of carbon monoxide is relatively complex as it is accompanied by the carbon deposition and the formation of intermediate carbides. The main carbon deposition reactions involved are

$$2\ CO_{(g)} \leftrightarrow C_{(s)} + CO_{2(g)} \quad (16)$$

$$CO_{(g)} + H_{2(g)} \leftrightarrow C_{(s)} + H_2O_{(g)} \quad (17)$$

It should be noted that Equation (7)–(15) results in a weight loss for the sample while Equation (16) and (17) cause a net weight gain. Equation (16) is known as the Boudouard reaction[16] and plays a crucial role in iron oxide reduction. Carbon monoxide tends to decompose into carbon dioxide at a certain low temperature and deposit carbon. Equation (16) and (17) are responsible for carbon deposition when H_2/CO mixtures are used as reducing gases. Which reactions among these two will dominate in the carbon deposition process depends on the H_2 concentration.[17] A detailed discussion will follow in the last part of this article. But from a naked eye perspective, it is understandable that adding H_2 will push the equilibrium of reaction 17 toward the right. This will produce more deposited carbon. However, it is not wise to come to a decision barely from the chemical reactions, as other factors like temperature play a huge role. The carbon produced at low temperatures has a twofold effect: 1) reducing the iron oxide as an indirect reduction process as given by Equation (13)–(15), where carbon reduces the iron oxides to iron. However, this reduction with carbon is relatively slow[18] and 2) depositing as soot might have negative aftereffects, as will be seen later.

Table 1. Iron ore reduction states and associated theoretical weight loss.

Reaction states	Weight loss	Equation no.
$Fe_2O_3 \rightarrow Fe_3O_4$	3.34%	(7),(10),(13)
$Fe_3O_4 \rightarrow FeO$	6.91%	(8),(11),(14)
$FeO \rightarrow Fe$	22.28%	(9),(12),(15)

A lot of experimental studies in the literature[10–12,19] mentioned the presence of cementite through carburization. Therefore, Equation (18)–(20) is specifically included to model the carbide formation

$$Fe_{(s)} + (2/3)\ CO_{(g)} \rightarrow (1/3)\ Fe_3C_{(s)} + (1/3)\ CO_{2(g)} \quad (18)$$

$$3\ Fe_{(s)} + C_{(s)} \leftrightarrow Fe_3C_{(s)} \quad (19)$$

$$Fe_3C_{(s)} + 2\ H_{2(g)} \leftrightarrow 3\ Fe_{(s)} + CH_{4(g)} \quad (20)$$

The iron oxide reduction process and the carbide formation take place simultaneously, as the cementite is present in partially reduced samples.[19] Investigating the solid species evolution with time in our model also shows similar insights.

A detailed reduction mechanism including methane submechanism will be published in due course. Under practical conditions, the water–gas shift reaction ($CO_{(g)} + H_2O_{(g)} \leftrightarrow H_{2(g)} + CO_{2(g)}$) could be an interesting possibility while using H_2/CO mixtures. In an actual shaft reactor, as the pellets will be in an atmosphere containing these product gases (H_2O, CO_2), this has important consequences on the required reduction time. However, for lab-scale experiments where insignificant amounts of product gases are available, this reaction has almost no effects. Hence, it is not included in our current reaction scheme.

2.3. Thermodynamics of Carbon Deposition and Cementite Formation

The range of gas compositions and temperatures over which carbon deposition is expected depends on the thermodynamic of that system. Therefore, a thermodynamic analysis of carbon deposition and cementite formation serves as an initial screening for a proposed kinetics reaction scheme. From thermodynamic considerations, the reduction with hydrogen should always be done at the highest possible operating temperature due to the expansion of the stable iron regime. However, the scenario with CO reduction is different; as the temperature decreases, iron's stability regime increases and the reducing gas utilization decreases. However, due to economic and kinetic limitations, an optimal operating temperature needs to be maintained for a better reduction degree. A Baur–Glässner diagram for the Fe–O–C–H system has been illustrated in **Figure 1**. It shows the

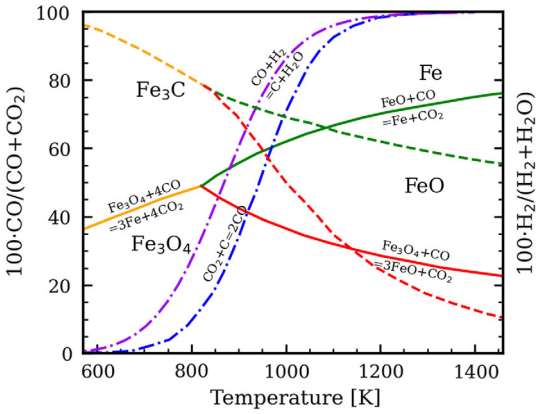

Figure 1. Chaudron (or Baur–Glässner diagram) phase diagram of Fe–O–C–H system. The solid lines represent the Fe–O–C system, while dashed lines represent the Fe–O–H system. The green and red lines/dashed lines illustrate wüstite and magnetite reduction, respectively. The orange line/dashed line represents the reduction of magnetite to iron at a temperature lower than 843 K. The blue and violet dashed dotted lines correspond respectively to the Boudouard reaction and to the $CO_{(g)} + H_{2(g)} = C_{(s)} + H_2O_{(g)}$ reaction at 1 atmospheric pressure.

thermodynamically most stable iron phases under variation of CO or H_2 content in CO/CO_2 or in H_2/H_2O atmospheres and the temperature. Carbon deposition mainly takes place at the surface of the pellet and under certain conditions (reducing gas concentrations, the total pressure in the reactor, residence time, and temperatures). However initially, carbon could also deposit inside the pellet, and as time progresses, a dense layer of soot will prevent further deposition inside. Eventually, the deposition rate is high enough to influence the overall conversion degree. This carbon layer hinders the availability of the reducing gas inside the pellet resulting in an incomplete reduction and a weight gain of the sample.[11] It can be seen in Figure 1 that the Boudouard reaction line crosses the wüstite reduction reaction line at 971 K. So on the left side area of this line, CO will be converted to CO_2, and carbon will start to deposit. It was also reported in DR experiments[19] that carbon deposition started significantly at 973 K and below. As the reduction progresses, the carbon deposition continues to form on the surface, creating a layer, which eventually hinders the diffusion of reductant inside the pellet. This deposition process will go on until 1273 K; afterward, regardless of the gas composition, there could be practically no further carbon deposition found on the pellet surface.[11] Cementite is relatively stable in a temperature range of 973 and 1123 K.[12,19] After 1223 K the cementite fraction in the sample will start to decompose.[19]

2.4. Parameters Estimation

The model employs a certain number of parameters that are detailed in the following subsections. Among these parameters, some are unknown and need to be estimated. To this end, the least square method has been employed. Starting from an initial set of parameters, the system of ODEs is solved and the global conversion degrees obtained from the model are compared to the experimental data. The parameters are then fit to minimize the sum of the squares of the deviations. To avoid overfitting issues, the number of parameters to fit is kept as low as possible. A unique set of chemical parameters is used for all experiments. An additional unknown parameter, the tortuosity, is related to the intrinsic properties of the pellets and was also kept constant when several experiments utilize the same pellet. More details are given in the following.

2.4.1. Activation Energies and Rate Constants

Despite having numerous studies on the kinetic parameters and their use in scaling up reactors, reliable kinetic parameters are not yet available. Gas–solid reaction kinetics is inherently complex compared with homogeneous reaction kinetics as they can rarely be explained by a single n^{th} order algebraic equation over the entire reaction range. The geometrical considerations are one of the most critical experimental factors that introduce considerable deviations[20] in the measured frequency factor (A) and activation energy (E_a) for a particular reaction. Therefore, considering the usual energy barrier model of homogeneous chemical reactions is not suitable. Instead the apparent activation energy is used. The Arrhenius relation is used to calculate the rate constants (k) of the reduction reactions.

$$k = A\, e^{\left(\frac{-E_a}{RT}\right)} \tag{21}$$

From the literature, it can be seen that the variation in E_a is wide. Spreitzer et al.[21] summarized the apparent activation energy proposed by different research groups. They showed that the range of apparent energy varies from 30 to 246 kJ mol^{-1} for $Fe_2O_3 \rightarrow Fe_3O_4$. For the reaction states of $Fe_3O_4 \rightarrow FeO$, the values are in the range between 33 and 47 kJ mol^{-1}. Moreover, for the most important states of the reduction process, $FeO \rightarrow Fe$, it varies from 11 to 85 kJ mol^{-1}. This value depends on material characteristics, gas compositions, operating temperature, grain size, material impurities, and the types of the experiments.

The determination of the kinetic parameters of the mechanism presented in Section 2.2 has been achieved sequentially. For example, experiments utilizing pure hydrogen involve only the three reduction reactions (Equation (7)–(9)). The kinetic parameters of these three reactions were determined on this reduced set of experiments. Similarly, experiments utilizing only carbon monoxide have supported the optimization of the chemical parameters of the reactions that do not involve hydrogen. Finally, the remaining reactions (Equation (17) and (20)) were fit based on syngas cases. One simplification has been made; though the reduction from magnetite to wüstite and from wüstite to iron is by nature reversible, it is not possible from the current available experimental setups to calculate separately the reverse reaction rates from the forward rates. The reverse reactions simply slow down the forward ones, so that both forward and backwards rates are lumped in apparent forward rates. A similar issue arises while trying to fit the individual step of the reduction as every step takes place simultaneously and this is coupled with transport effects. For these reasons, the choice was made to only fit forward rates for the reduction and to employ a common activation energy for a same reducing agent. After optimization, the activation energies found for the reduction with H_2 and CO for all the three reduction steps in this work are 75 and 65 kJ mol^{-1}, respectively.

2.4.2. Porosity

The porosity affects the reduction process considerably. Most of the previous works either considered it as constant or modeled it using linear correlations with too many empirical coefficients. However, considering empirical coefficients for each solid oxides, which also change for different pellet types (fired pellet, nonfired pellet, sintered) makes the model overfitted. In this work, the initial porosity is taken from the corresponding author and later discretized and solved along the radius of the pellet.

$$\frac{\partial \varepsilon}{\partial t} = -\sum_j \frac{M_j}{\rho_j} \dot{s}_j \tag{22}$$

In this way, our model considers the porosity variation with the time and along the radius without prior assumptions.

2.4.3. Effective Diffusivity

The bulk diffusivity of each gaseous species is calculated using Cantera[22] to obtain the mixture-averaged diffusion coefficients (D_{coeff}) [$\text{m}^2\,\text{s}^{-1}$] relating the molar diffusive fluxes to gradients in the species mole fractions. As the diffusion of gaseous species through porous solid depends on the porosity, the tortuosity, and the pore size distribution,[23] the effective diffusivity (D^{eff}) is calculated by the following equation

$$D^{\text{eff}} = (\varepsilon/\tau)\, D_{\text{coeff}} \tag{23}$$

where, ε and τ represent the pellet's porosity and tortuosity, respectively. Some of the researchers also include Knudsen diffusivity to calculate the effective diffusivity.[7] Molecular and Knudsen diffusion usually coexist and it is essential to consider both effects, when the pores in the porous materials are in the nanometer range. However, as the pores in the industrial pellets are not very fine and reduction operations are carried out at atmospheric pressure, the Knudsen diffusion term is not considered here.[24] As the morphology of pellet sample varies from one research group to another, the tortuosity values of the pellets for different research groups are not comparable. For a pellet sample of similar initial porosity used by a research group, the tortuosity values are the same. (e.g., Bonlade et al.[25] in **Table 2** carried out three experiments with a pellet porosity of $\varepsilon = 22\%$; as the values of the initial porosity used by the group are the same, the tortuosity factor values are kept identical; here, $\tau \approx 6.3$). There are certain analytical expressions (e.g., Bruggeman correlation) relating the porosity to the tortuosity factor to describe transport in porous media. This type of correlation often includes arbitrary indices that need to be fitted. So, to avoid such unwanted complexity, the tortuosity factor is directly optimized to fit the experimental data.

2.4.4. Mass Transfer Coefficient

Many mathematical models made a simplified assumption of neglecting external mass transfer. The general claim is that when the gas flow rate is greater than 1 Nl/min, external mass transfer is not a rate-limiting factor anymore. However, Kazemi et al.[26] show that the gas flow rate has specific effects on the overall conversion degree. In this work, the mass transfer coefficient (k_{coeff}) is also considered for the gas film resistance and optimized for each experimental case.

2.5. Literature Experimental Data Sets

Several experimental data from different research groups have been considered to validate the proposed generic mechanism. The literature data considered here focus on the reduction of spherical hematite pellets, and the reducing gases are H_2 and CO at atmospheric pressure, eventually in the presence of other gas species (He, CO_2, CH_4). A summary of the isothermal experimental data sets is listed in Table 2. The traditional experimental setup for studying the kinetics of gaseous reduction of iron ore is the thermogravimetric analyzer (TGA). Though the similar term "TGA" has been used when referring to the experimental process by almost all the research groups, the techniques of starting the reduction process are quite different. In a usual TGA setup, the sample is heated in inert atmosphere to the desired reduction temperature. Then the inert gas is switched to the reducing gas to start the reduction process. This process involves a comparatively longer time to reach the desired reduction temperature, and the uncertainty of initial gas composition can affect the overall reduction process. The group of Kazemi et al.[26] introduced a new type of TGA setup with a cooling chamber on top of the reaction tube. The sample can be moved up and down to introduce it into the reaction chamber to start the reduction process or to retract it to the cooling chamber to stop it immediately. The TGA setup can also differ in terms of reducing gas introduction. For example, the group Beheshti et al.[27] used a concentric walled crucible where the reducing gases are heated through their way to the down while passing in between the walls. In this technique, the opening of the inlet port at the bottom of the concentric crucible is large enough not to build up any pressure. While passing through the concentric wall these gases will also be heated uniformly. Other research groups like Mousa et al.[10] used a system consisting of a vertical Tammann furnace with a layer of alumina ball at the bottom to get a uniform flow of reducing gas. All the research groups considered here generally used industrial pellets for the experiments. There are some uncertainties in the data listed here, for example, data from Beheshti et al.[27] show quite a bit of irregularity in the trend. Some data from Towhidi et al.[11] demand further discussions.

3. Results and Discussions

In order to better understand the chemical and the transport processes of a hematite pellet reduced in a gaseous environment, the present model has been validated against the literature data listed in Table 2. The global conversion degree (F) is the main validation criterion for the model and is defined as

$$F = \frac{m_0 - m(t)}{m_0 - m_f} \tag{24}$$

where $m(t)$ is the instantaneous weight of the solid during the reduction process. The parameters m_0 and m_f represent the

Table 2. Summary of the experimental data from the literature (atmospheric pressure).

Author	Gas composition (H_2/CO/CH_4/CO_2)	Reduced material Fe_2O_3/FeO/Gangue	Temperature [K]	Porosity [%]	Flow rate [Nl/min]	Diameter [mm]
Beheshti et al.[27]	0.444/0.556/0/0	0.971/0/0.029	1173	27	2	11.00
	0.545/0.455/0/0		1173			
	0.616/0.384/0/0		1173			
	0.667/0.333/0/0		1173			
Kazemi et al.[28]	Pure H_2	0.96/0.04/0	1123	19	1	11.00
			1073	34		
			1123	34		
			1073	26		
			1123	26		
Patisson et al.[29]	0.6(0.4 He)	0.971/0/0.029	973	33	2	14.00
			1073			
			1173			
			1223			
Kazemi et al.[26]	0.5/0.5/0/0/0	0.96/0.04/0	1123	27	2	11.00
	0.6/0.4/0/0/0		1123			
	0.667/0.333/0/0		1123			
	0.8/0.2/0/0		1123			
	0.5/0.5/0/0		1123			
Towhidi et al.[11]	Pure H_2	0.96/0.04/0	878	15.8	–	15.20
			973			14.98
			1173			15.30
			1253			15.30
			1507			15.24
Towhidi et al.[11]	Pure CO	0.96/0.04/0	878	15.8	–	15.20
			973			14.98
			1173			15.30
			1253			15.30
			1507			15.24
Towhidi et al.[11]	0.5/0.5/0/0	0.96/0.04/0	878	15.8	–	15.20
			970			14.90
			1059			15.28
			1173			15.12
			1253			14.84
			1507			14.40
Towhidi et al.[11]	0.25/0.75/0/0	0.96/0.04/0	973	15.8	–	15.02
			1046			15.10
			1173			15.30
			1507			15.24
Towhidi et al.[11]	0.75/0.25/0/0	0.96/0.04/0	973	15.8	–	15.00
			1059			15.06
			1173			15.30
			1507			15.28
Bonlade et al.[25]	Pure H_2	0.967/0.017/0.016	1173	22	2	10.70
	Pure CO		1173			
	0.557/0.340/0.04/0.063		1173			

initial weight of the pellet and the theoretical weight after complete reduction.

3.1. Reduction Behavior of Hematite with Pure H_2 or Pure CO

The reduction behaviors of hematite in pure H_2, diluted H_2, or pure CO atmospheres are shown in **Figure 2**.

Except at 878 K, where experimental data at a later stage are missing, all cases with pure H_2 (Figure 2a,b) show a conversion degree (F) of hematite higher than 98% at the end. From Figure 2a, it is visible that, with increasing temperatures, the rate of conversion degree $\left(\frac{dF}{dt}\right)$ also increases. Another observation is that a higher porosity of the sample contributes to a higher conversion degree. Overall, the model is well responsive to the temperature variation or the pellet porosity. The cases involving hydrogen diluted in helium (Figure 2c) are also well rendered by the simulations. The dilution of hydrogen logically slows down the reduction process. For example, the full conversion

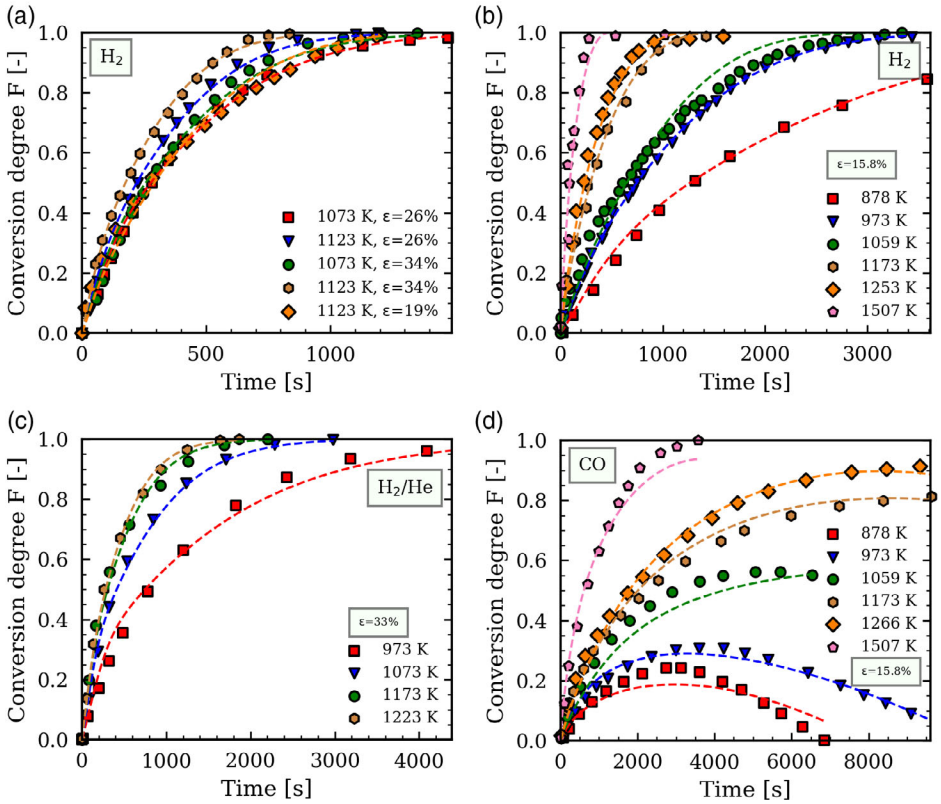

Figure 2. Reduction behavior of hematite pellet using pure H_2 or diluted H_2 (40% Helium) or pure CO as reducing gas versus time. Dashed lines and symbols represent the current model simulation and the experimental data from the literature, respectively. Literature data considered are a) Kazemi et al.,[28] b,d) Towhidi et al.,[11] and c) Patisson et al.[29] ε represents the pellet porosity, and the pellet characteristics are given in Table 2.

is obtained at about 3000 s at 1073 K in the diluted case, while it was 1300 s for a pellet featuring almost similar porosity in the pure hydrogen case. Based on these results, the choice of the transport modeling and of the partial order of 1 with respect to hydrogen seems adapted.

The reduction with pure carbon monoxide in Figure 2d shows different profiles. The hematite sample is clearly visible to be converted to the highest degrees at shorter retention times with pure H_2. At 1507 K, the experimental results with pure CO show complete conversion while the present model reaches a maximum below the complete conversion. The iron ore reduction modeling at high (above 1300 K) temperature is relatively an uncharted territory. This very high process temperature might involve additional chemical pathways, cracking, or swelling of the sample not considered here. Most importantly, the DR processes are usually carried out approximately at a temperature range of 1073–1373 K.[30] In Figure 2d, two examples illustrate the direct reduction at these intermediate temperatures (1173 and 1266 K). The conversion degree reaches a plateau below 1, whose value depends on the temperature. In these cases, the pellet can be totally converted, but the presence of carbon, mainly in cementite form, accounts for additional weight, not considered in the theoretical weight after the complete reduction that appears in the conversion degree term. Furthermore, at temperatures below 1059 K, the hematite reduction (weight loss) and carbon deposition (weight gain) are competing processes, which explain the shape of the curves and render the problem more complex. Considering this, deviations from the experiments while modeling carbon deposition phenomena are to be expected.

3.2. Reduction Behavior of Hematite with Syngas (H_2/CO)

The reduction with syngas ($H_2 + CO$) is not as straightforward as with H_2, rather associated with other submechanisms (like carbon deposition, Fe_3C formation, gasification reactions, etc.), which make it difficult to establish a model for a wide range of experimental conditions. **Figure 3** shows the conversion degree (F) against the retention time for various gas compositions ($r = H_2$:CO molar ratio). From these two graphs, it is evident that with increasing H_2 content, the conversion degree of the sample also increases but does not reach 100% conversion like the reduction with H_2 in Figure 2a,b. This is due to the carburization of reduced iron into cementite (Fe_3C) in the later stage of reduction. In Figure 3b, the model shows some disagreements with the data because the experimental setup used by the author could not produce consistent data and the uncertainties in those data are quite high. **Figure 4** illustrates the sensitivity of the operating temperature on the total conversion degree. With increasing operating temperatures, the rate of conversion $\left(\frac{dF}{dt}\right)$, as well as the final conversion degree also increased.

An interesting trait is that, similar to the reduction with CO, when the reducing temperatures are lower than 1059 K, the

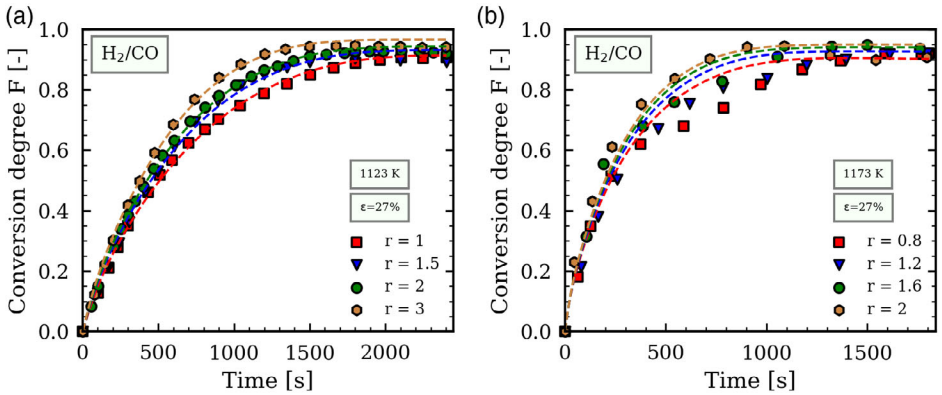

Figure 3. Influence of the gas composition on the reduction behavior of hematite pellet using syngas (H_2/CO) versus time. Dashed lines and symbols represent the current model simulation and the experimental data from the literature, respectively. Literature data considered are a) Kazemi et al.[26] and b) Beheshti et al.[27]. ε and r represent the pellet porosity and H_2:CO ratio and the pellet characteristics are given in Table 2.

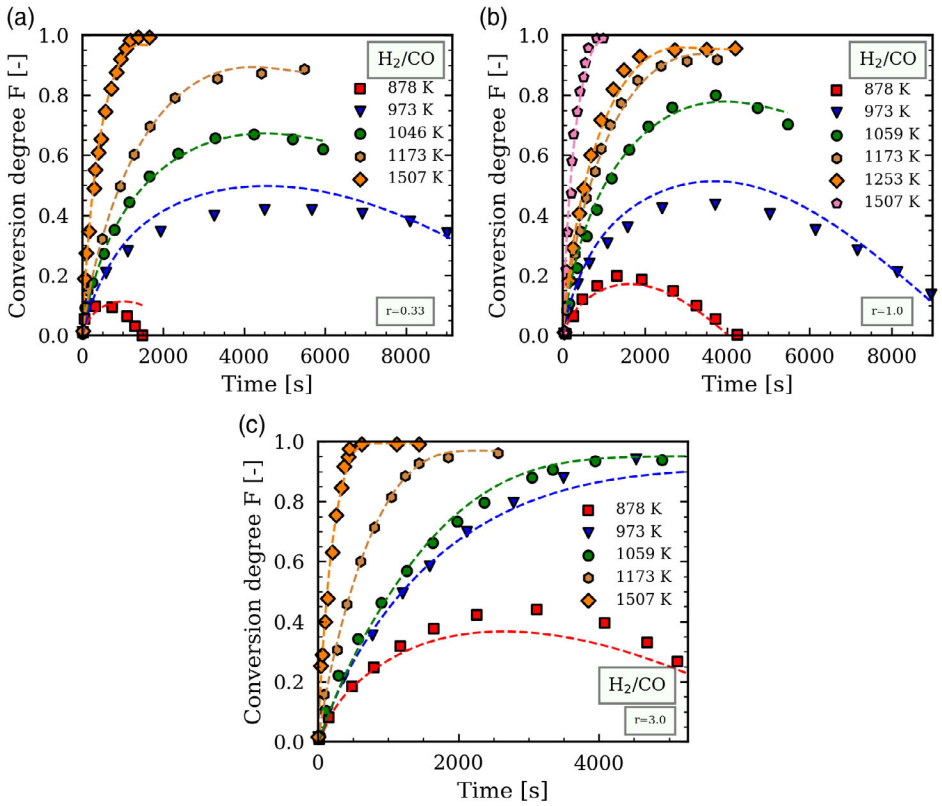

Figure 4. Effect of the temperature on the reduction behavior of hematite pellet using syngas (H_2/CO) versus time. Dashed lines and symbols represent the current model simulation and the experimental data from the literature, respectively. Literature data (a, b, and c) are taken from Towhidi et al.[11] ε and r represent the pellet porosity and H_2:CO ratio, and the pellet characteristics are given in Table 2.

reduction proceeds to a certain maximum conversion degree and then the conversion curve starts to go down. This negative slope in the conversion degree curve represents a net weight gain of the pellet. This is due to the mass of carbon depositing that overcomes the mass of iron oxide that reduces. Extreme cases of carbon deposition are experienced with $r = 0.33$. Our model reproduces those traits quite well. Surprisingly, the experimental test case at 973 K in Figure 4c reaches a higher final conversion degree than the case at 1059 K. There might be a bias in these specific experimental data, as it contradicts all other observations. Based on that, the difference at 973 K between the simulated result and experimental data at the end is well justified.

3.3. Effects of Varying Reducing Gas Composition

In the steel-making community, a growing interest has been observed in reducing iron ore using pure hydrogen. Several key factors must be investigated while transitioning the

steelmaking process towards hydrogen. Those are chemical kinetics, thermodynamics, or heat transfer effects. Regarding the chemical kinetics on the reduction of iron ore using H_2, CO, and syngas, at a constant temperature, **Figure 5**a (here at $T = 1173$ K) clearly shows that the kinetics of H_2 is the fastest, then followed by syngas, and then CO. To investigate which reactions play a major role, a sensitivity analysis has been done; the analyses were performed at a conversion degree of 55% to serve as an example. The sensitivity coefficient (S_n) for the n^{th} reaction in the reaction scheme is calculated as follows.

$$S_{\mathrm{n}} = \frac{F_t^{\mathrm{Sens}} - F_t}{F_t} \times 100 \tag{25}$$

Here, F_t and F_t^{Sens} represent the global conversion degree (F) at a particular time t and the global conversion degree achieved at the same time, when the reaction rate (k_n) of the n^{th} reaction is increased or decreased by a certain amount. In our case, we tested the sensitivity by increasing and decreasing the reaction rates by 10%.

The reduction with pure H_2 involves only three reactions, and as it could be expected, FeO→Fe reaction is the most dominating reaction. The two other reaction rates are not rate limiting in the process and have therefore a limited impact on the conversion degree. For the reduction with CO, as we can see clearly from Figure 5c, no reaction overpasses the others. The sensitivity of the Boudouard reaction (carbon deposition) is of the same magnitude as the reduction step FeO → Fe with CO, but with the opposite sign. The main reactions that reduce the oxides are challenged parallelly by the carbon deposition, characterized by a final conversion degree much lower than 1. The syngas sensitivity analysis in Figure 5d clearly indicates that the $FeO + H_2 \rightarrow Fe + H_2O$ and $FeO + CO \rightarrow Fe + CO_2$ reactions are the major reactions. Cementite formation reactions show quite a minor sensitivity, in accordance with the low amount of carbon that the final conversion seems to indicate. This figure also shows that at this temperature and syngas composition rich in hydrogen, the process is mostly dominated by the reduction.

Figure 6a tackles the impact of the gas composition and temperature on the conversion rates. The initial conversion rates at a given H_2/CO ratio divided by the conversion rates with pure CO at a certain temperature T are shown in Figure 6, where each line corresponds to a different temperature of reference.

From the kinetic point of view, the conversion rates using 100% hydrogen is up to 7 times faster than the conversion rates using CO. This is also experimentally reported by several researchers.[23,25] It is well known that hydrogen always acts as a better reducing agent: it is more reactive with the oxides and diffuses faster than CO.[9] However, the present study allows for a quantification of these phenomena. The gas composition has a more limited impact at lower temperatures. As the reduction of iron oxide with H_2 is thermodynamically not favored at lower temperature (□−973 K and Δ−1059 K) the values of the $\mathrm{rate}_{(H2/CO)}$:rate_{COT} in Figure 6a do not vary much with the increase in H_2 content in the reducing gas. A key aspect is that the increase is not linear. The increase is limited between the H_2: CO gas ratio of 25:75 and 75:25 but rises near pure hydrogen conditions (Figure 6a). This rise might be explained by the

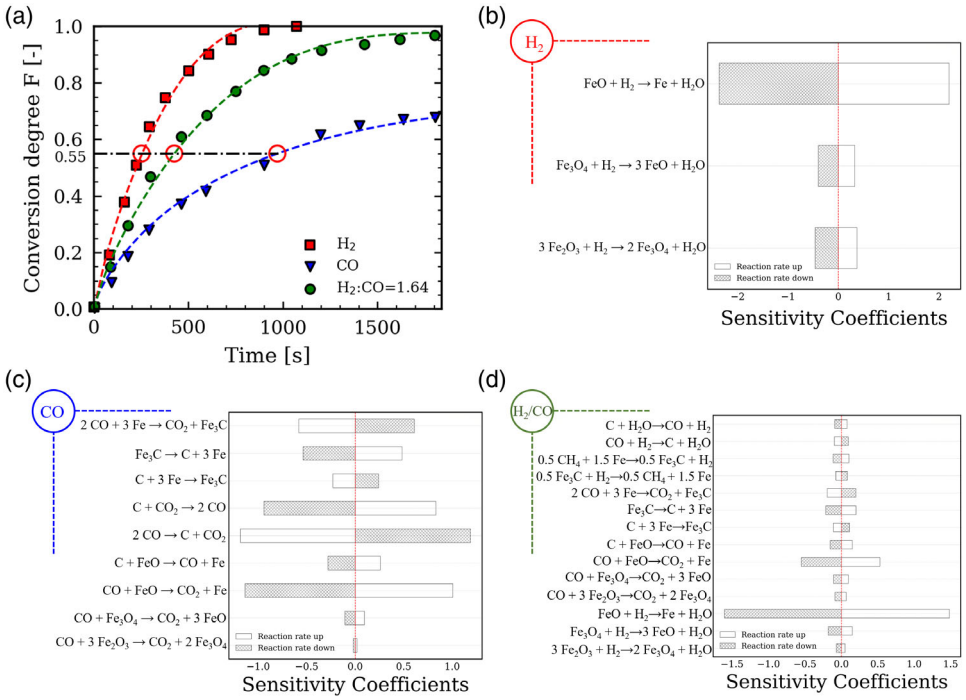

Figure 5. Sensitivity analysis of chemical reactions in the reduction process with H_2, CO, and syngas; all at $T = 1173$ K. a) Comparison of the reduction behavior using pure H_2, pure CO, and syngas. The experimental data are taken from Bonlade et al.[25] A horizontal dashed-doted line (-.-) at 55% conversion indicates where the sensitivity analysis has been performed. b,c,d) Sensitivity analysis at 55% conversion degree with H_2, CO, and syngas, respectively.

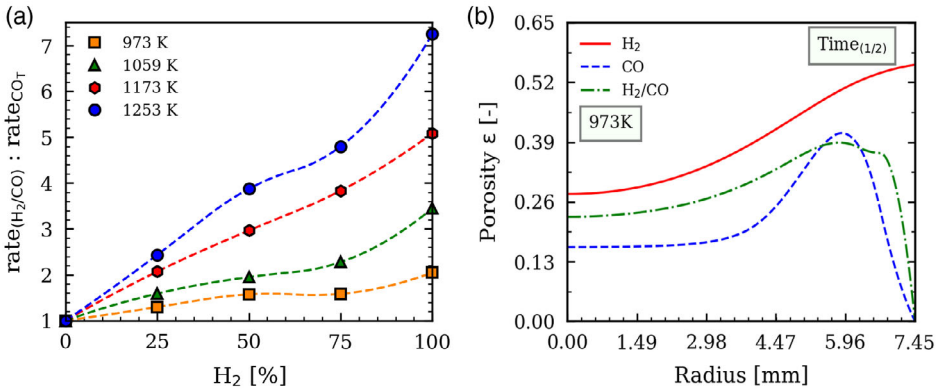

Figure 6. a) Calculated initial conversion rates relative to the conversion rates of pure CO at 973, 1059, 1173, and 1253 K as a function of the H_2 content in the H_2/CO-mixtures. b) Variation of calculated pellet porosity (initial porosity: 15.8) across the pellet radius at the half time ($t_{(1/2)}$) of the reduction process using H_2, CO, and H_2/CO (50:50) at 973 K.

complete absence of carbon deposition in pure hydrogen cases, which would enable the transport of the reducing agent to the oxide sites, in addition to the better diffusivity and reactivity of hydrogen. Another considerable effect of varying gas compositions on the reduction behaviour of iron oxide is the evolution of the pellet porosity across the radius. Figure 6b illustrates the structural changes during the reduction process, more specifically the porosity for various gas compositions at the half time of the reduction process at 973 K. The initial porosity of the pellet for all these three cases is 15.8%. The case with pure hydrogen is easier to apprehend. The process is governed by the step-wise reduction of hematite to iron, and the absolute density of iron is greater than the one of the oxides. As the pellet volume is kept constant and the reduction starts from the surface, the porosity is maximum near the surface and lower toward the core of the pellet. At the end of the complete conversion, the porosity reaches up to 60%. This goes in line with the experimental investigation of Towhidi et al.,[11] who concluded that the pellet porosity increases considerably during the reduction process. They measured an initial pellet porosity of 15.8% and a porosity after reduction using H_2 of about 61.0%. The profiles of the syngas and CO cases are different. The porosity increase due to the reduction is counterbalanced by the carbon that deposites, especially on the surface. The two chosen cases illustrate extreme carbon deposition cases. The porosity approaches zero, which stops the diffusion inside the pellet. At this point, the only process going on is carbon depositing on the surface as it does not require internal transport. In real experiments, the layer of carbon is growing with time. Our model only considers constant pellet size, but it was sufficient to reproduce these cases with important carbon deposition.

3.4. Carbon Deposition and Cementite Formation

In DR processes, hematite reduction reactions occur simultaneously with the carburization reactions.[11] However, at a certain stage, the rate of carburization reactions (carbon deposition and cementite formation reactions) exceeds the rate of reduction reactions. From that point onward, the pellet gains weight due to cementite formation and the carbon deposition. At which stage and to what extent, the carburization reactions will outplay the reduction reactions depend on several experimental conditions. Before going further with the chemistry of the carburization process, a schematic illustration of the process is presented in **Figure 7** to investigate these phenomena.

The process starts with the reduction of the hematite with reducing gas. As the reduced iron appears on the pellet's surface, it starts to react with the available carbon/–CO/–CH_4 to form the cementite (Fe_3C). This carbon is produced through the Boudouard reaction. As the formation of the cementite grows on the surface, the reduction process slows down. With time, the surface of the pellet will be saturated with cementite. At this stage, the carbon produced by the Boudouard reaction will start to deposit on top of the cementite layer. This dense layer will prevent the reducing gas from diffusing through the pellet and eventually stop the reduction process. From then, the pellet

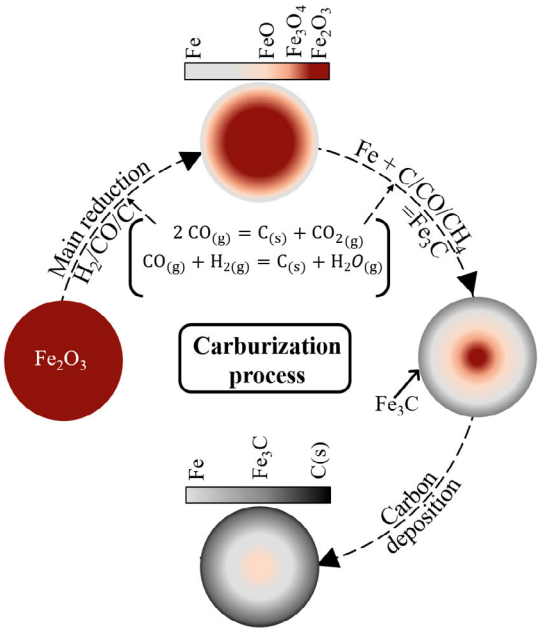

Figure 7. Schematic of the carburization process.

starts to gain weight due to soot formation. Carbon deposition is mainly controlled by the temperature, pressure, CO concentration, and nature of the solid surface.[11] After reproducing a large number of experimental data, our model gives us enough confidence to use it as a tool to analyze the data regarding carburization. In **Figure 8**a, the rate of carbon formation along the time for several temperatures using 50:50 H_2:CO gas composition is calculated. The highest initial carbon formation rate is observed at 878 K, and as the operating temperature increases, this rate decreases. At 1173 K, negligible amounts of carbon form in the system. Another important aspect: the rate of carbon formation increases until a certain time for all the operating temperatures. Then, the carbon formation rate becomes almost steady. This nature of carbon formation can be explained like this.

1) Carbon is formed through the Boudouard reaction and Equation (17). Hence, the lower the operating temperature, the higher the rate of carbon formation. 2) The rate of carbon formation is initially lower because the available carbon in the system will be consumed for a certain time through a) reducing the iron oxide and b) converting the reduced iron to cementite. 3) As the pellet surface is saturated with Fe_3C, the carbon formation rate becomes steady. From this point, carbon formed in the system will start to deposit on the pellet's surface.

Another observation in Figure 8a is that the time required to stabilize the rate of carbon formation varies for different temperatures. The lower the operating temperature, the longer it will take to reach a steady formation of carbon. This is due to the slower reduction of iron oxide at lower temperatures so that the formation of the cementite and saturation of the surface takes a longer time. An important factor affecting carbon deposition is the concentration of H_2 in the H_2/CO mixtures.[17] In Figure 8b, the effect of the gas composition on carbon deposition is presented. The rate of carbon deposition in this figure is calculated at around 50 min. It is due to the observation from Figure 8a, where the carbon formation rate stabilizes on an average after 50 min. Hydrogen presence in the reducing gas mixture promotes carbon deposition. However, when the H_2 percentage in the reducing gas mixture is higher than 50%, the carbon deposition reduces drastically. These findings were also experimentally reported by Turkdogan et al.[17]

The reason could be that at low H_2:CO ratios, the carbon deposition is obtained not only from the Boudouard reaction, but also because of Equation (17), $CO_{(g)} + H_{2(g)} = C_{(s)} + H_2O_{(g)}$. At higher H_2 content, the contribution of the Boudouard reaction becomes limited, and as H_2 is participating more in the reduction, more H_2O is produced, which pushes the equilibrium of Equation (17)

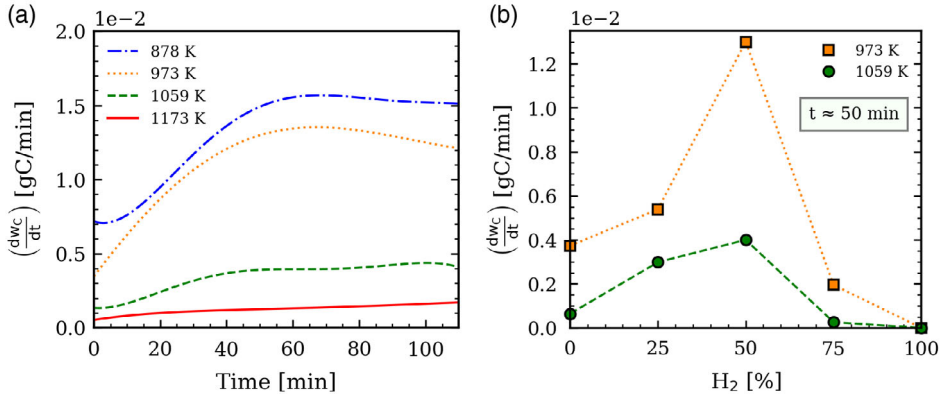

Figure 8. Simulated model analysis of a) rate of carbon formation along the reduction process for H_2:CO = 50:50 and b) effects of gas composition and temperature on the rate of carbon deposition in H_2/CO mixtures at around 50 min.

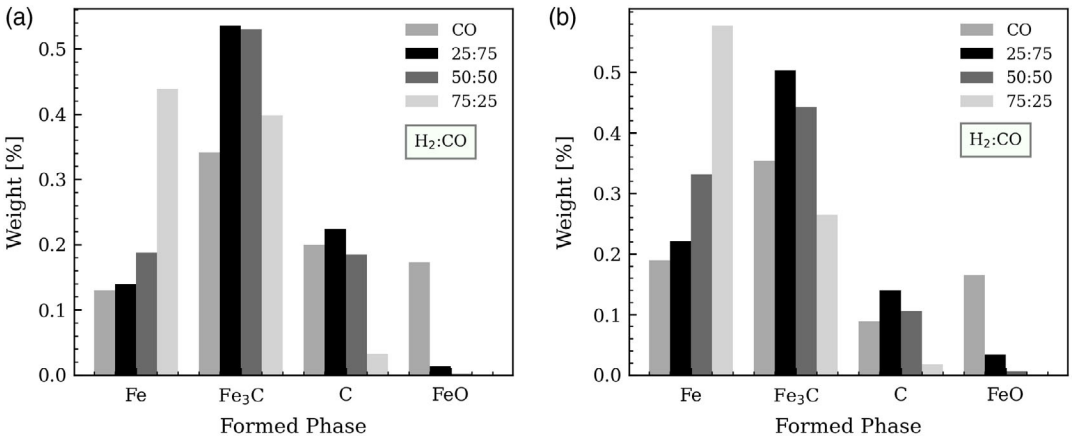

Figure 9. Quantitative analysis of the different species developed in the 55% reduced pellets with different gas compositions at a) 973 K and b) 1059 K.

from right to left. The formation of cementite can be directly correlated with the amount of carbon deposition. A qualitative analysis of Fe, FeO, Fe_3C, and C will shed more light on the discussion. In **Figure 9**, a comparative quantitative analysis between 973 and 1059 K temperature for different reducing gas mixtures is shown for a 55% reduced sample. If we compare these two figures, we can clearly see that, more reduced iron is available for all the gas mixtures at higher temperature as higher temperature promotes faster reduction reactions. The amount of cementite formed at 1059 K is lower than the temperature of 973 K for all the gas compositions. The deposited carbon at the temperature of 973 K is clearly higher than the temperature of 1059 K. Increasing H_2 content in the reducing gas mixture affects the growth of the cementite and carbon deposition in a positive way up to a certain degree. The highest amount of cementite formation is calculated using H_2:CO = 25:75 for both temperatures.

4. Conclusion

A kinetic model has been proposed which is sufficiently generic to successfully predict the direct reduction process of a single hematite spherical pellet for a wide range of conditions like the porosity, the temperature, the pellet size, or the gas compositions with high accuracy. The kinetic mechanism is supported by a reduction model that includes the variation of porosity with time and the consideration of mass transfer limitations in the gas phase. On this basis, the kinetic model also shows maturity in predicting complex carbon deposition phenomena. The differences between the reduction using CO, syngas, and H_2 are discussed in light of thermodynamics and chemical kinetics. At the end, the carburization kinetics is explained schematically. Sensitivity of temperature and gas compositions on carbon deposition and cementite formation are discussed. Our calculated results to explain the carburization process are aligned with the thermodynamic considerations and comforted by similar trends and results reported in the literature. This better understanding will help to support the development of DR processes with flexible reducing agent compositions, up to pure hydrogen.

Acknowledgements

Open Access funding enabled and organized by Projekt DEAL.

Conflict of Interest

The authors declare no conflict of interest.

Data Availability Statement

The data that support the findings of this study are available from the corresponding author upon reasonable request.

Keywords

carburization, direct reduction processes, H_2/CO reduction, iron oxide pellets, porous solid model

Received: January 13, 2022
Revised: June 16, 2022
Published online:

[1] C. P. Manning, R. J. Fruehan, *JOM* **2001**, *53*, 36.
[2] World Steel Association, *World Steel in Figures 2020*, www.worldsteel.org (accessed: December 2021).
[3] IEA, *Iron and Steel Technology Roadmap*, www.worldsteel.org (accessed: December 2021).
[4] World Steel Association, *Steel's Contribution to A Low Carbon Future and Climate Resilient Societies—World Steel Position Paper*, www.worldsteel.org (accessed: December 2021).
[5] W. M. Mckewan, *Trans. Metal. Soc. AIME.* **1961**, *224*, 2.
[6] Q. T. Tsay, W. H. Ray, *ISIJ Int.* **1976**, *22*, 1064.
[7] M. S. Valipour, M. Y. Motamed Hashemi, Y. Saboohi, *Adv. Powder Technol.* **2006**, *17*, 277.
[8] E. T. Turkdogan, J. V. Vinters, *Metal. Trans.* **1971**, *2*, 3175.
[9] H. B. Zuo, C. Wang, J. Dong, K. Jiao, R. Xu, *Int. J. Miner. Met. Mater.* **2015**, *22*, 688.
[10] E. A. Mousa, A. Babich, D. Senk, *Steel Res. Int.* **2013**, *84*, 1085.
[11] N. Towhidi, J. Szekely, *Metall. Mater. Trans. B* **1983**, *14*, 359.
[12] P. X. Ming-Wei, J. B. J. Jesse, *J. Am. Ceram. Soc.* **1989**, *72*, 110.
[13] Q. Fradet, M. L. Ali, U. Riedel, *Steel Res. Int.* **2021**, 2200042.
[14] J. O. Edström, *J Iron Steel Res. Int.* **1953**, *175*, 289.
[15] M. I. A. Heidari, N. Niknahad, T. Fabritius, *Materials* **2021**, *14*, 7450.
[16] O. C. R. Boudouard, *Acad. Sci. Paris* **1899**, *128,* 824.
[17] E. T. Turkdogan, J. V. Vinters, *Metal. Trans.* **1974**, *5,* 11.
[18] T. I. Kang, *MSc. dissertation, The University of New South Wales*, **2000**.
[19] M. Kazemi, Du Sichen, *Metall. Mater. Trans. B* **2016**, *47,* 3519.
[20] M. Maciejewski, *J. Therm. Anal.* **1992**, *38*, 51.
[21] D. Spreitzer, J. Schenk, *Steel Res. Int.* **2019**, *90*, 1900108.
[22] D. G. Goodwin, R. L. Speth, H. K. Moffat, B. W. Weber, *Cantera: An object-oriented software toolkit for chemical kinetics, thermodynamics, and transport processes*, https://www.cantera.org/, **2021**, Version 2.5.1.
[23] N. Towhidi, *Ironmaking Steelmaking* **1981**, *6*, 237.
[24] C. Strangfeld, *Adv. Eng. Mater.* **2021**, *23*, 2100106.
[25] A. Bonalde, A. Henriquez, M. Manrique, *ISIJ Int.* **2005**, *45*, 1255.
[26] M. Kazemi, B. Glaser, D. Sichen, *Steel Res. Int.* **2014**, *85*, 718.
[27] R. Beheshti, J. Moosberg-Bustnes, R. E. Aune, in *TMS 2014: 143rd Annual Meeting & Exhibition*, Springer, Cham, Switzerland, **2016**.
[28] M. Kazemi, M. S. Pour, D. Sichen, *Metall. Mater. Trans. B* **2017**, *48*, 1114.
[29] F. Patisson, O. Mirgaux, *Metals* **2020**, *10*, 922.
[30] Y. Takenaka, Y. Kimura, K. Narita, D. Kaneko, *Comput. Chem. Eng.* **1986**, *10*, 67.